Plasmonic Intravascular Photoacoustic Imaging for Detection of Macrophages in Atherosclerotic Plaques

ARTICLE *in* NANO LETTERS · NOVEMBER 2008

Impact Factor: 13.59 · DOI: 10.1021/nl801852e · Source: PubMed

NANO LETTERS

2009
Vol. 9, No. 6
2212-2217

Plasmonic Intravascular Photoacoustic Imaging for Detection of Macrophages in Atherosclerotic Plaques

Bo Wang,† Evgeniya Yantsen,† Timothy Larson,† Andrei B. Karpiouk,† Shriram Sethuraman,† Jimmy L. Su,† Konstantin Sokolov,†,‡ and Stanislav Y. Emelianov*,†

Department of Biomedical Engineering, University of Texas at Austin, Austin, Texas 78712, Departments of Biomedical Engineering and Imaging Physics, University of Texas M.D. Anderson Cancer Center, Houston, Texas 77030 USA

Received June 26, 2008; Revised Manuscript Received September 15, 2008

ABSTRACT

To detect macrophages in atherosclerotic plaques, plasmonic gold nanoparticles are introduced as a contrast agent for intravascular photoacoustic imaging. The phantom and ex vivo tissue studies show that the individual spherical nanoparticles, resonant at 530 nm wavelength, produce a weak photoacoustic signal at 680 nm wavelength while photoacoustic signal from nanoparticles internalized by macrophages is very strong due to the plasmon resonance coupling effect. These results suggest that intravascular photoacoustic imaging can assess the macrophage-mediated aggregation of nanoparticles and therefore identify the presence and the location of nanoparticles associated with macrophage-rich atherosclerotic plaques.

Every year, cardiovascular disease claims more lives in United States than any other disease including cancer.[1] Despite advances in determining risk factors and treating myocardial infarction, there are few techniques available for imaging the development of the atherosclerotic plaques that play a major role in cardiovascular disease. Macrophages are one of the key components involved in the pathology of atherosclerosis. At a relatively early stage in atherosclerotic development, macrophages are present at the "crime scene": macrophages are formed from the blood monocytes that enter the arterial wall because of the initial inflammation in the arterial endothelial layer. During the progression of the disease, lipid-laden macrophages play a partial role in the formation of atheroma.[2,3] Macrophage infiltration into the fibrous cap of plaques also accelerates disease progression by causing the release of matrix metalloproteinases (MMPs),[4] which weaken the fibrous cap and make the plaques prone to rupture.[5] Clearly, the distribution and activity of macrophages provide important information on the development of atherosclerotic plaques. Therefore, it is important to develop robust and cost-effective imaging methods sensitive to the cellular composition of plaques.

With almost any imaging technique, imaging the macrophages requires a contrast agent. Therefore, different types of contrast agents have to be introduced in various imaging methods, such as magnetic resonance imaging (MRI), computed tomography (CT), optical coherence tomography (OCT) and ultrasound imaging, to image macrophage distribution.[6−9] Nanoparticles have been widely used as a contrast agent to image macrophages by MRI and OCT since macrophages endocytose particles into intracellular vesicles. The imaging contrast is enhanced by the high local concentration of contrast agents in macrophages. For example, in optical imaging, gold nanoparticles (Au NPs) become an ideal contrast agent because of their biocompatibility and high optical scattering coefficients.[10−15] Moreover, the optical spectra of Au NPs can be tuned by changing the size and/or shape of the particles,[16] thus providing flexibility in different applications.

Recently, intravascular photoacoustic (IVPA) imaging, a catheter-based, minimally invasive imaging technique, was introduced to image atherosclerosis.[17] Generally, photoacoustic imaging is a technique to ultrasonically image the optical absorption of tissue. Specifically, the tissue is irradiated with a short laser pulse, and photoacoustic transients are generated as the light is absorbed in tissue. These acoustic waves, recorded using an ultrasound sensor, are used to form an image. The differences in optical absorption among arterial tissue components provide contrast in IVPA imaging. Using a laboratory prototype of the IVPA imaging system consisting of a pulsed laser source and an

* To whom correspondence should be addressed. Telephone: (512) 471-1733. Fax: (512) 471-0616. E-mail: emelian@mail.utexas.edu.
† University of Texas at Austin.
‡ University of Texas M.D. Anderson Cancer Center.

10.1021/nl801852e CCC: $40.75
Published on Web 10/10/2008

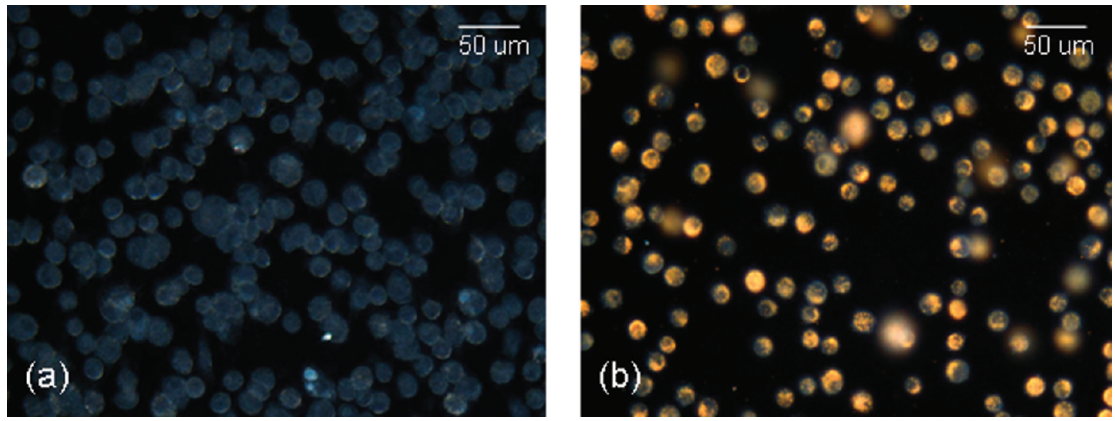

Figure 1. Darkfield reflectance optical images of intact murine macrophages (left) and murine macrophages loaded with gold nanoparticles (right). The images were obtained using Xe illumination and a 20× darkfield objective (0.5 NA) with Leica 6000 DM upright microscope.

intravascular ultrasound (IVUS) imaging catheter, the ability of IVPA imaging to detect atherosclerotic plaques was demonstrated.[17] Furthermore, the IVPA imaging has the potential to differentiate between plaques of different compositions.[18]

IVPA imaging has high spatial resolution and sufficient imaging depth for detecting atherosclerosis. Compared to noninvasive cardiovascular imaging modalities such as MRI and CT, IVPA imaging can achieve higher spatial resolution. Indeed, IVPA resolution is on the order of tens of micrometers as opposed to larger than 300 μm in MRI[19] or 400 μm in CT.[7] Compared to invasive but high resolution imaging modalities such as OCT, IVPA has a larger penetration depth of several millimeters relative to 1−2 mm imaging depth in OCT.[20] In addition, by choosing the imaging wavelengths in the near-infrared (NIR) range where the optical absorption of oxygenated and deoxygenated blood is low, IVPA imaging may be performed in the presence of luminal blood.[21] Finally, since an IVUS imaging catheter is used in the IVPA imaging system, coregistered ultrasound and photoacoustic imaging of the vessel cross-section is possible; the combined IVPA/IVUS image shows both the structure and optical absorption properties of the imaged object.

Because of their high optical absorption coefficient, different types of Au NPs with surface plasmon resonance characteristics tuned to a specific spectral range have been used as contrast agent in photoacoustic imaging.[22−25] In this work, we explore the ability of IVPA imaging to detect macrophages using plasmonic nanoparticles as contrast agents. The ability to accurately detect the distribution of the macrophages with high specificity can aid in identifying vulnerable plaques at clinically relevant stages of disease progression.[26]

Fifty nanometer diameter spherical Au NPs were synthesized via citrate reduction of $HAuCl_4$ under reflux.[27] To passivate the surface of NPs, the NPs were coated with methoxy-polyethylene glycol-thiol (mPEG-SH); a small volume of 10^{-4} M mPEG-SH solution (MW 5000 kD, Shearwater) was added to the gold suspension and allowed to react for 30 min on shaker. After incubation, a small volume of 2% PEG polymer (MW 15 kD, Sigma) was added to the mixture as a surfactant to prevent aggregation of NPs during centrifugation.

Mouse monocytes−macrophages (J774A.1 cell line) are characterized by a high rate of nonspecific uptake, similar to most cells of a macrophage phenotype. Cells were cultivated in DMEM supplemented with 5% FBS at 37 °C in 5% CO_2. To load cells with gold nanoparticles, macrophages were incubated with a suspension of PEGylated nanoparticles (approximately 4×10^{10} particles/ml) in phenol red free and serum free DMEM overnight (Figure 1). To determine the uptake of nanoparticles by microphages, the number of particles internalized by cells and the number of cells were measured. Specifically, the optical density of the incubating medium was measured at 530 nm wavelength before and after incubation, and the values of optical density were compared with the optical density of standard Au NP solutions at 530 nm wavelength to calculate the number of particles internalized by cells. Macrophages were counted using a hemocytometer. The concentration of particles per cell was determined by dividing the number of internalized nanoparticles by the number of cells. Finally, six samples with a similar number of cells incubated with the same number of nanoparticles were prepared and analyzed to evaluate the precision of the concentration measurements. The results showed that the number of particles per cell is consistent across multiple samples with a value of $(1.82 \pm 0.06) \times 10^4$ particles per cell.

The extinction spectra of NP suspension, macrophages, and macrophages loaded with NPs were measured using a UV−vis spectrometer (BioTek). The extinction spectrum of macrophages loaded with NPs was obtained by subtracting its extinction spectrum from the extinction spectrum from the same concentration of macrophages only. Normalized extinction spectra of NP suspension and macrophages loaded with NPs are shown in Figure 2. The suspension of spherical gold nanoparticles has an extinction peak at 530 nm, whereas cells loaded with nanoparticles have an extinction peak around 540 nm. Furthermore, the extinction peak of cells loaded with particles is broader than the peak of NP suspension. The red-shift and broadening of the extinction spectrum are attributed to plasmon resonance coupling of

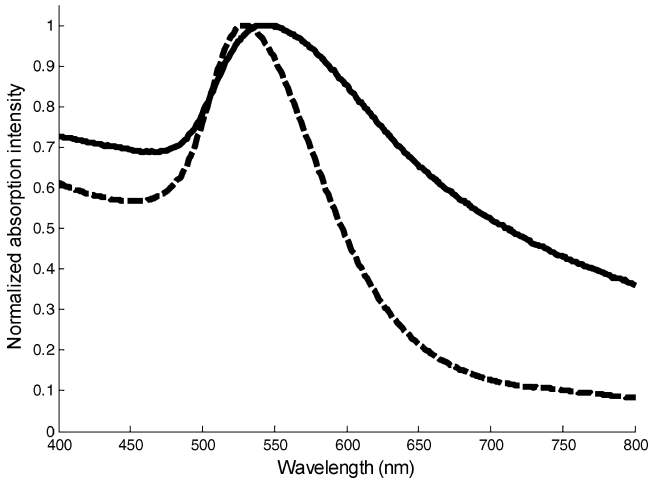

Figure 2. Normalized extinction spectra of macrophages loaded with Au NPs (solid line), and Au NPs only (dashed line). Both absorption spectra were normalized with their corresponding maxima.

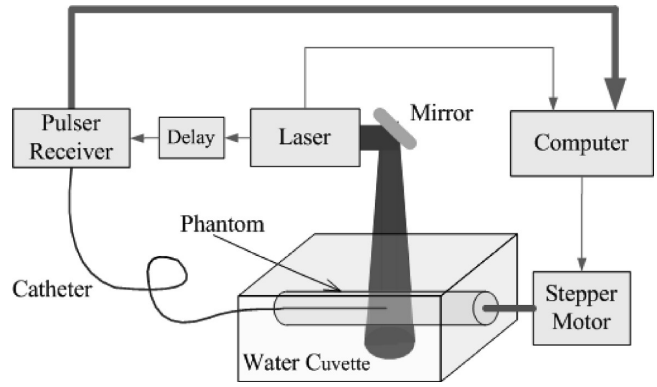

Figure 3. Intravascular photoacoustic (IVPA) and intravascular ultrasound (IVUS) imaging system setup.

nanoparticles inside the macrophages[11,13,28] and demonstrate that the NPs internalized by macrophages are aggregated within the cells.

A tissue mimicking phantom was made to test whether Au NPs can be used as a contrast agent in IVPA imaging. To simulate the arterial wall, a 25 mm long and 6 mm diameter cylindrical tube was made out of 8% polyvinyl alcohol mixed with 0.4% silica by weight to mimic the optical and acoustic scattering properties of muscle or collagen in the arterial wall.[29] Within the phantom wall, four compartments near and around the lumen were created. Each of the four compartments was filled with 10% gelatin gel containing either (1) Au NPs (2×10^{11} nanoparticles per ml), (2) gelatin only, (3) murine macrophages loaded with Au NPs ($1 \times 10^4 - 6 \times 10^4$ nanoparticles per cell with the total concentration of 2×10^{11} nanoparticles per ml), or (4) murine macrophages without Au NPs. The last two compartments, containing an equal number of cells, simulated the macrophage-rich atherosclerotic plaques before and after the intravenous injection and subsequent uptake of Au NPs by the microphages. In this phantom, the PVA and gelatin gel simulates healthy tissue, and the compartment with Au NPs suspended in gel represents the circulating Au NPs.

The diagram of the IVUS/IVPA imaging system is presented in Figure 3. During imaging, the sample was placed in a water cuvette filled with saline. The IVPA images of the phantom were obtained using either an Nd:YAG laser operating at 532 nm wavelength or an OPO laser system tunable within 680−750 nm. Both laser systems produced 4−7 ns pulses. The fluences of the laser irradiation were around 7 mJ/cm^2 at 532 nm wavelength and 10 mJ/cm^2 at 680 nm wavelength. The photoacoustic signals generated by each laser pulse were collected with a 40 MHz single element transducer of the IVUS imaging catheter (Boston Scientific, Inc.) inserted into the lumen of the modeled vessel. After a 9 μs delay, an ultrasound signal was generated and received by the same transducer. Once the photoacoustic and ultrasound signals were acquired, the sample was rotated around the longitudinal axis to a new angular position using a stepper motor. As the phantom was rotated 360°, coregistered IVUS and IVPA images of the vessel's cross-section were collected.

The combined IVUS/IVPA imaging of the phantom was first performed at 532 nm wavelength to confirm the content in each compartment. Then, the same cross-section of the phantom was imaged at 680 nm wavelength to demonstrate the red-shift effect caused by the plasmon resonance of Au NPs. The IVUS, IVPA, and combined IVUS/IVPA images of the same cross-section of the phantom are shown in Figure 4. Images presented in Figure 4 panels b and c were collected at 532 nm wavelength, and images in Figure 4 panels e and f were collected at 680 nm. In the IVUS image (Figure 4d), the compartments filled with macrophages are characterized by the presence of a weak echo signal (small intensity of grayscale ultrasound). Neither gelatin nor Au NPs affect contrast in ultrasound images; low concentrations of Au NPs cannot be seen directly from IVUS images. At 532 nm wavelength (Figure 4b), both isolated Au NPs and the nanoparticles aggregated inside of the macrophages have high contrast in the IVPA image. However, the IVPA image alone may not provide sufficient anatomical or structural information. By combining the IVUS and IVPA images (Figure 4c), the location of Au NPs can be identified and the composition in each compartment can be further inferred. At 680 nm wavelength (Figure 4e), only the compartment filled with NP-loaded macrophages produces photoacoustic signal. This is due to the elevated absorption of aggregated NPs at this wavelength (Figure 2). In contrast, the signal from the compartment filled with suspended Au NPs is very weak and below the noise level of the imaging system. The high strength of photoacoustic signal received from the aggregated NPs compared to the photoacoustic signal from both non-aggregated and suspended NPs suggests that only Au NPs internalized by the macrophages will provide contrast in clinical IVPA imaging performed using 680 nm wavelength. Indeed, the photoacoustic response from macrophages is enhanced once the Au NPs are endocytosed. At the same time, the IVPA imaging at this wavelength can be used to avoid imaging of nonaggregated Au NPs, such as NPs circulating in the luminal blood. Finally, imaging in this spectral range reduces the influence of optical absorption of luminal blood.

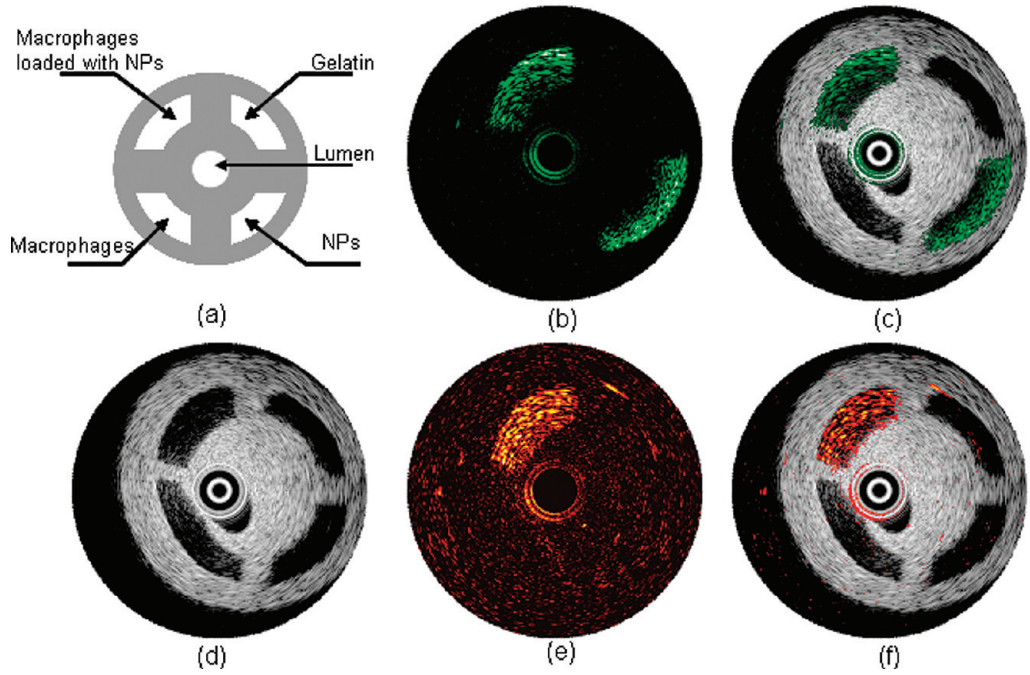

Figure 4. The diagram (a) and the IVUS image (d) of the tissue mimicking phantom. The dynamic ranges of IVUS and IVPA images were 50 and 17 dB, respectively. The IVPA images of the same cross-section of the phantom were taken at 532 nm (b) and 680 nm wavelength (e). The combined IVUS and IVPA images of the phantom (panel c, 532 nm wavelength and panel f, 680 nm wavelength) indicating the origin of the photoacoustic responses in IVPA images.

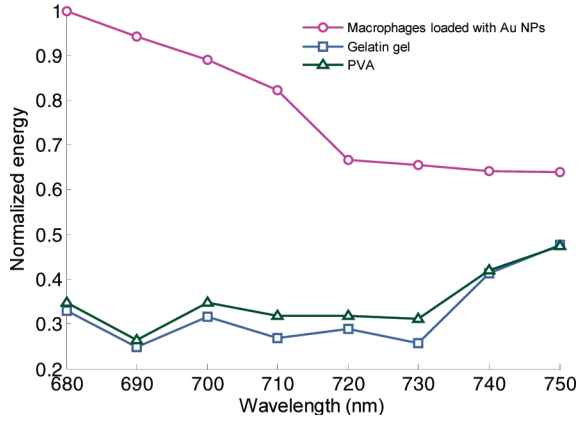

Figure 5. Strength of the photoacoustic signal at different wavelength measured from the small regions containing macrophages loaded with Au NPs, gelatin gel, and PVA. Each spectrum is normalized to the maximum signal strength from Au NPs loaded macrophages at 680 nm wavelength.

Multiwavelength IVPA imaging was performed to confirm the presence of aggregated particles and to differentiate labeled macrophages from other tissue constituents such as red blood cells or lipids. The phantom was imaged every 10 nm within the 680−750 nm wavelength range. Figure 5 shows the quantitative behavior of the wavelength-dependent photoacoustic response from specific parts of the phantom: macrophages loaded with Au NPs, 10% gelatin, and PVA. The highest normalized energy of the IVPA signal was detected from NP-loaded macrophages at 680 nm wavelength. As the wavelength increases, the IVPA signal amplitude from NP-loaded macrophages decreases. This measurement qualitatively correlates with the direct measurements of absorption spectrum from labeled macrophages (Figure 2). In contrast, the photoacoustic response from gelatin gel and PVA is much lower and increases with the increased optical wavelength. This trend of increasing strength of the photoacoustic signal with increasing wavelength can help to differentiate NP loaded macrophages from the background. Since the absorption spectra of various arterial tissues such as blood, fat and muscle behave differently from aggregated Au NPs at wavelengths from 680 to 750 nm,[30] labeled macrophages can be distinguished by multiwavelength IVPA imaging.

To further demonstrate that IVPA imaging with Au NPs can be used for imaging of macrophages in atherosclerotic plaques, ex-vivo tissue experiments were performed on a diseased rabbit aorta. A section of the aorta was extracted from a rabbit that was on a high cholesterol diet for 3 months. Macrophages loaded with Au NPs (approximately 4×10^4 nanoparticles per cell) were mixed with gelatin (2×10^7 cells per ml) and injected into the outer and inner boundary of the aorta. The sample was imaged by the same IVPA/IVUS imaging system used in phantom experiments. The hypoechoic regions in the IVUS image, denoted by green arrows in Figure 6a,b,e, indicate the areas of the injection of macrophages loaded with Au NPs. IVPA images of this cross-section were taken at 700, 750, and 800 nm wavelengths. As shown in Figure 6, Au NPs produce the strongest photoacoustic signal when irradiated with laser pulses at 700 nm wavelength. At a laser fluence of 15 mJ/cm^2, the particles produce readily detectable photoacoustic signal from the laser light traveling through more than 1 mm of the arterial tissue. As the wavelength increased, the photoacoustic signal strength from Au NPs decreased; the photoacoustic response is hardly visible at 800 nm wavelength. This decreasing trend

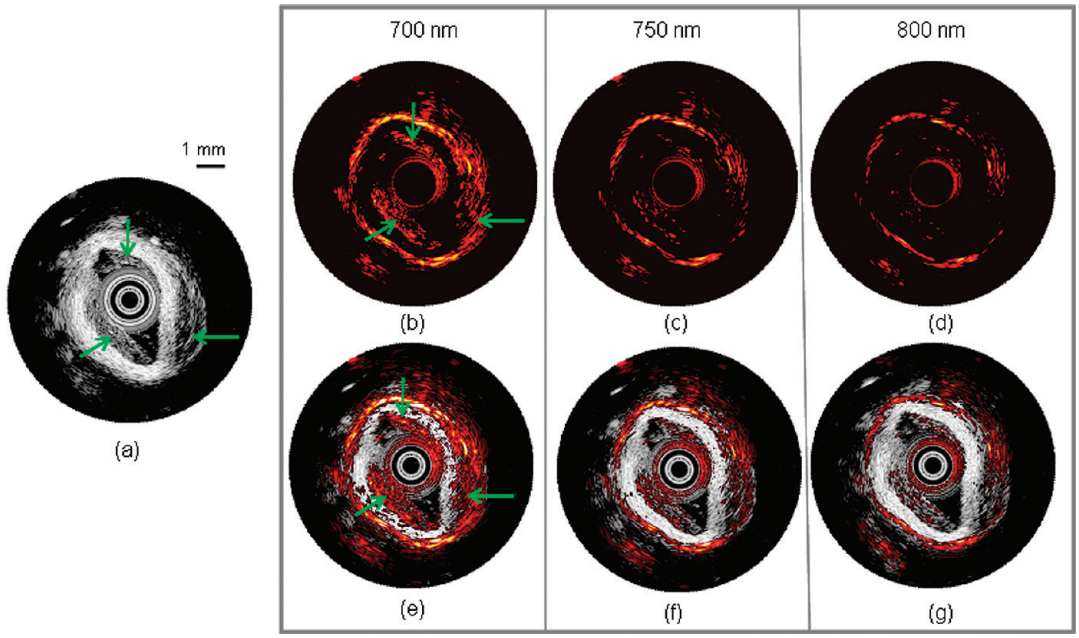

Figure 6. IVUS, IVPA, and combined IVUS/IVPA images of a diseased rabbit aorta injected with macrophages loaded with Au NPs. The IVUS image (panel a) is displayed using 50 dB dynamic range. The injected macrophages in the outer and inner regions of aorta are denoted in the images (a,b,e) with green arrows. The normalized IVPA images (panels b−d) and combined IVUS/IVPA images (panels e−g) obtained using 700, 750, and 800 nm wavelength are displayed using 20 dB display dynamic range. The IVPA and combined IVUS/IVPA images taken at 700 nm wavelength (panels b,e) showed high photoacoustic signal at the injected regions denoted by arrows.

of photoacoustic signal magnitude closely corresponds to the absorbance spectra of aggregated Au NPs. Therefore, the ex vivo tissue experiment demonstrates the ability of IVPA imaging to detect macrophages loaded with Au NPs.

In this study, solid gold nanospheres were used. Besides the nanoparticles with solid gold cores, particles can be manufactured with other core materials and then coated with gold. Such particles can serve as the contrast agent for multimodal imaging. For example, gold-coated iron nanoparticles[31−33] can be used for both photoacoustic imaging and MRI imaging. Moreover, the extinction spectra of these particles can potentially be tuned by changing the thickness of the gold coating; this approach has been applied for tuning the optical properties of gold nanoshells consisting of a silica core and a gold shell.[34] A major advantage of using spherical Au NPs as contrast agents for IVPA imaging is that the photoacoustic signal from NPs suspended in luminal blood can be avoided. Because the suspended particles do not produce detectable photoacoustic signal in the NIR spectral region, photoacoustic imaging at 680 nm wavelength can be performed immediately after the administration of particles to monitor the uptake of nanoparticles within the macrophages. In addition, using photoacoustic imaging at another wavelength (i.e., 532 nm wavelength for 50 nm spherical Au NPs), particle circulation half-life can possibly be assessed. Therefore, the photoacoustic imaging of the atherosclerosis can be performed when the optimum concentration of nanoparticles in plaques is reached.

While this study observed that Au NPs were passively taken up by macrophages, Au NPs can be functionalized with antibodies to target different types of plaque constituents. For example, photoacoustic imaging of cancer cells has been performed at the molecular level by using functionalized spherical Au NPs to target EGFR receptors of cancer cells.[25] Similarly, IVPA imaging can utilize functionalized Au NPs to target constituents closely related to plaque progression. For example, the development of vasa vasorum, which is neovasculature formed in the outer region of the atherosclerotic vessel wall, is known to be associated with the growth of atherosclerotic lesions and is closely related to plaque vulnerability. Specifically, Au NPs can be functionalized to target $\alpha_v\beta_3$ integrin involved in atherosclerosis progression and expressed highly in vasa vasorum.[35] Since the diameter of blood vessels in the vasa vasorum is small, and the blood vessels are located relatively deeply within the media-adventitia layer, IVPA imaging is a promising candidate to image the vasa vasorum.

In our initial experiments, where a single layer of NP-loaded macrophages was irradiated with 50 laser pulses at 680 nm wavelength with a fluence up to 114 mJ/cm^2, no cell death was observed. Generally, however, due to the high optical absorption of Au NPs compared to the other constituents in the artery, the heat deposition in the NP-targeted tissue can be increased dramatically and cause selective cell death.[36] Although current nanoparticle-based photothermal therapy approaches are focused on cancer treatment, Au NPs have the potential to be used in the photothermal therapy of vulnerable plaques.

In clinical studies, to deliver Au NPs to the macrophages located in the artery, nanopartcles have to penetrate through the endothelial cells in the intima layer. Nanoparticles that are small in size can more easily enter the intima of the arterial wall. However, at the same time, the particle size needs to be in a certain range to achieve maximum cellular uptake.[37] Therefore, further studies are needed to find the optimal size of nanoparticles suitable for IVPA imaging of

macrophages. Furthermore, in our laboratory experiments, the tissue samples were irradiated from the outside using a relatively simple optical delivery system. For in vivo applications, a combined imaging catheter capable of delivering the laser light into the lumen needs to be developed. A prototype of such a combined imaging catheter consisting of an IVUS imaging catheter integrated with a fiber optical light delivery system is being constructed and tested using tissue mimicing phantoms.

In summary, we demonstrated that the aggregation of Au NPs within the macrophages causes red-shift in the optical absorbance spectra. By utilizing elevated absorption due to plasmon resonance coupling, IVPA imaging at around 700 nm wavelength can detect the signal from macrophages enhanced by aggregated Au NPs. The difference between the aggregated and nonaggregated Au NPs provides a mechanism to identify the macrophages using Au NPs as contrast agents. Moreover, multiwavelength IVPA imaging can be used to differentiate photoacoustic signals from aggregated NPs and photoacoustic signals generated from the adjacent tissues. The phantom experiments and ex vivo studies suggest that IVPA imaging is a promising tool for detecting macrophages with plasmonic contrast agents.

Acknowledgment. We are grateful to Dr. Richard W. Smalling and James H. Amirian from University of Texas Health Science Center Houston for providing the excised samples of rabbit aorta. We also would like to acknowledge the in-kind support from Boston Scientific, Inc. This work was partially supported by the American Heart Association under Grant 0655033Y and National Institutes of Health under Grants EB004963 and HL084076.

Note Added after ASAP Publication: This paper was published ASAP on October 10, 2008. Shriram Sethuraman was added as a contributing author. The revised paper was reposted on May 6, 2009.

References

(1) American Heart Association; http://www.americanheart.org/presenter.jhtml?identifier=3038611
(2) Libby, P. *Nature* **2002**, *420*, 868–874.
(3) Hansson, G. K. *New Engl. J. Med.* **2005**, *352*, 1685.
(4) Galis, Z. S.; Sukhova, G. K.; Kranzhofer, R.; Clark, S.; Libby, P. *Proc. Natl. Acad. Sci. U. S. A.* **1995**, *92*, 402.
(5) Falk, E.; Shah, P. K.; Fuster, V. *Circulation* **1995**, *92*, 657–671.
(6) Kooi, M. E.; Cappendijk, V. C.; Cleutjens, K.; Kessels, A. G. H.; Kitslaar, P.; Borgers, M.; Frederik, P. M.; Daemen, M.; van Engelshoven, J. M. A. *Circulation* **2003**, *107*, 2453–2458.
(7) Hyafil, F.; Cornily, J. C.; Feig, J. E.; Gordon, R.; Vucic, E.; Amirbekian, V.; Fisher, E. A.; Fuster, V.; Feldman, L. J.; Fayad, Z. A. *Nat. Med.* **2007**, *13*, 636–641.
(8) Gobin, A. M.; Lee, M. H.; Halas, N. J.; James, W. D.; Drezek, R. A.; West, J. L. *Nano Lett.* **2007**, *7*, 1929–1934.
(9) Feinstein, S. B. *J. Am. Coll. Cardiol.* **2006**, *48*, 236–243.
(10) Yguerabide, J.; Yguerabide, E. E. *J. Cell. Biochem.* **2001**, *84*, 71–81.
(11) Sokolov, K.; Aaron, J.; Hsu, B.; Nida, D.; Gillenwater, A.; Follen, M.; MacAulay, C.; Adler-Storthz, K.; Korgel, B.; Descour, M. *Technol. Cancer Res. Treat.* **2003**, *2*, 491–504.
(12) Alivisatos, P. *Nat. Biotechnol.* **2004**, *22*, 47–52.
(13) Aaron, J.; Nitin, N.; Travis, K.; Kumar, S.; Collier, T.; Park, S. Y.; Jose-Yacaman, M.; Coghlan, L.; Follen, M.; Richards-Kortum, R. *J. Biomed. Opt.* **2007**, *12*, 034007.
(14) Aslan, K.; Lakowicz, J. R.; Geddes, C. D. *Curr. Opin. Chem. Biol.* **2005**, *9*, 538–544.
(15) Abrams, M. J.; Murrer, B. A. *Science* **1993**, *261*, 699–700.
(16) Link, S.; El-Sayed, M. A. *J. Phys. Chem. B* **1999**, *103*, 8410–8426.
(17) Sethuraman, S.; Aglyamov, S. R.; Amirian, J. H.; Smalling, R. W.; Emelianov, S. Y. *IEEE Trans. Ultrason. Ferroelectr. Freq.Control* **2007**, *54*, n/a.
(18) Sethuraman, S.; Amirian, J. H.; Litovsky, S. H.; Smalling, R. W.; Emelianov, S. Y. *Opt. Express* **2008**, *16*, 3362–3367.
(19) Fayad, Z. A.; Fuster, V. *Circ. Res.* **2001**, *89*, 305–316.
(20) Jang, I. K.; Bouma, B. E.; Kang, D. H.; Park, S. J.; Park, S. W.; Seung, K. B.; Choi, K. B.; Shishkov, M.; Schlendorf, K.; Pomerantsev, E. *J. Am. Coll. Cardiol.* **2002**, *39*, 604–609.
(21) Sethuraman, S.; Mallidi, S.; Aglyamov, S. R.; Amirian, J. H.; Litovsky, S.; Smalling, R. W.; Emelianov, S. Y. *Proc. SPIE* **2007**, *6437*, 643729–643721.
(22) Eghtedari, M.; Oraevsky, A.; Copland, J. A.; Kotov, N. A.; Conjusteau, A.; Motamedi, M. *Nano Lett.* **2007**, *7*, 1914–1918.
(23) Yang, X.; Skrabalak, S. E.; Li, Z. Y.; Xia, Y.; Wang, L. V. *Nano Lett.* **2007**, *7*, 3798–3802.
(24) Li, P. C.; Wei, C. W.; Liao, C. K.; Chen, C. D.; Pao, K. C.; Wang, C. R.; Wu, Y. N.; Shieh, D. B. *IEEE Trans. Ultrason. Ferroelectr. Freq. Control* **2007**, *54*, 1642–1647.
(25) Mallidi, S.; Larson, T.; Aaron, J.; Sokolov, K.; Emelianov, S. *Opt. Express* **2007**, *15*, 6583–6588.
(26) Chen, W. Q.; Zhang, L.; Liu, Y. F.; Chen, L.; Ji, X. P.; Zhang, M.; Zhao, Y. X.; Yao, G. H.; Zhang, C.; Wang, X. L. *Am. J. Physiol.: Heart Circ. Physiol.* **2007**, *293*, H2836.
(27) Brown, K. R.; Walter, D. G.; Natan, M. J. *Chem. Mater.* **2000**, *12*, 306–313.
(28) Rechberger, W.; Hohenau, A.; Leitner, A.; Krenn, J. R.; Lamprecht, B.; Aussenegg, F. R. *Opt. Commun.* **2003**, *220*, 137–141.
(29) Kharine, A.; Manohar, S.; Seeton, R.; Kolkman, R. G. M.; Bolt, R. A.; Steenbergen, W.; Mul, F. F. M. *Phys. Med. Biol.* **2003**, *48*, 357–370.
(30) Emelianov, S. Y.; Aglyamov, S. R.; Karpiouk, A. B.; Mallidi, S.; Park, S.; Sethuraman, S.; Shah, J.; Smalling, R. W.; J. M. Rubin, W. G. S. *Proc. - IEEE Ultrason. Symp.* **2006**, 405–415.
(31) Aaron, J. S.; Oh, J.; Larson, T. A.; Kumar, S.; Milner, T. E.; Sokolov, K. V. *Opt. Express* **2006**, *14*, 12930–12943.
(32) Lyon, J. L.; Fleming, D. A.; Stone, M. B.; Schiffer, P.; Williams, M. E. *Nano Lett.* **2004**, *4*, 719–723.
(33) Larson, T. A.; Bankson, J.; Aaron, J.; Sokolov, K. *Nanotechnology* **2007**, *18*, 325101.
(34) West, J. L.; Halas, N. J. *Annu. Rev. Biomed. Eng.* **2003**, *5*, 285–294.
(35) Hoshiga, M.; Alpers, C. E.; Smith, L. L.; Giachelli, C. M.; Schwartz, S. M. *Circ. Res.* **1995**, *77*, 1129–1135.
(36) Huang, X.; Jain, P. K.; El-Sayed, I. H.; El-Sayed, M. A. *Lasers Med Sci* **2008**, *23*, 217–228.
(37) Chithrani, B. D.; Chan, W. C. W. *Nano Lett.* **2007**, *7*, 1542–1550.

NL801852E